

Giant-spin nonlinear response theory of magnetic nanoparticle hyperthermia: a field dependence study

M. S. Carrião,* V. R. R. Aquino, and A. F. Bakuzis
Instituto de Física, Universidade Federal de Goiás, 74690-900, Goiânia-GO, Brazil

G. T. Landi
*Departamento de Ciências Naturais e Humanas,
Universidade Federal do ABC, 09210-580, Santo André-SP, Brazil*

E. L. Verde
Instituto de Ciências Exatas e da Terra, Universidade Federal de Mato Grosso, 3500, Pontal do Araguaia-MT, Brazil

M. H. Sousa
Faculdade de Ceilândia, Universidade de Brasília, 72220-140, Brasília-DF, Brazil

(Dated: February 8, 2017)

Understanding high-field amplitude electromagnetic heat loss phenomena is of great importance, in particular in the biomedical field, since the heat-delivery treatment plans might rely on analytical models that are only valid at low field amplitudes. Here, we develop a nonlinear response model valid for single-domain nanoparticles of larger particle sizes and higher field amplitudes in comparison to linear response theory. A nonlinear magnetization expression and a generalized heat loss power equation are obtained and compared with the exact solution of the stochastic Landau-Lifshitz-Gilbert equation assuming the giant-spin hypothesis. The model is valid within the hyperthermia therapeutic window and predicts a shift of optimum particle size and distinct heat loss field amplitude exponents. Experimental hyperthermia data with distinct ferrite-based nanoparticles, as well as third harmonic magnetization data supports the nonlinear model, which also has implications for magnetic particle imaging and magnetic thermometry.

Keywords: magnetic nanoparticles, hyperthermia, cancer, nonlinear, alternating magnetic field

I. INTRODUCTION

The response of nanomaterials to alternating electromagnetic fields is of great importance nowadays in the biomedical field, where new approaches to treat diseases are under development. One of the most innovative and important applications is related to heat delivery through the interaction of nanomaterials with electromagnetic fields. This heat delivery method can be used to release drugs[1], activate biological processes[2–4] and even treat tumors[5–9]. Indeed, using Maxwell’s equations and the first law of thermodynamics one finds that the heat loss per unit volume per cycle is given by

$$\frac{1}{V} \oint_{\text{cycle}} \delta Q = \int \vec{E} \cdot \vec{J} dt - \oint_{\text{cycle}} \vec{P} \cdot d\vec{E} - \oint_{\text{cycle}} \mu_0 \vec{M} \cdot d\vec{H}, \quad (1)$$

where V is the nanomaterial volume, Q is the heat loss, \vec{E} the electric field, \vec{J} the free volumetric density current, \vec{P} the electric polarization, μ_0 the vacuum magnetic permeability, \vec{M} the magnetization and \vec{H} the magnetic field. The first term in equation (1) correspond to the “free-current” loss, whereas the last two describe dielectric and magnetic losses.

Moreover the “free-current” loss term has an important impact on the biomedical application since it is related to a biological constraint. This term states that the fre-

quency (f) and magnitude of the alternating magnetic fields need to be lower than a critical value in order to inhibit possibly harmful ionic currents in the patient’s body[7]. For instance, for a frequency of 100 kHz the maximum field amplitude is in the order of 20.8 kA/m (261 Oe) for a single air-core coil radius of 0.035 m (expected dimension for breast cancer application[10]). Note that this value is higher than the one usually reported (order of 4.9 kA/m) only because the estimation of Atkinson used a coil radius of 0.150 m. Since the free current loss is proportional to the square of the distance from the coil axis, an estimation of the critical field for a given coil radius (r) might be obtained from $Hf < (0.150/r) * 4.85 \times 10^5$ kA/(m \times s). Figure 1 shows the biological critical field as a function of field frequency in the usual therapeutic hyperthermia range using Atkinson’s criteria[7, 10, 11], which indicates that the higher the frequency the lower is this field (the parameters used to generate the curve are presented in the figure captions).

On the other hand, the last terms of Eq. (1), which represent hysteretic losses, has been the subject of analytical models within the Linear Response Theory (LRT) and was used to estimate optimal particle size, understand particle-particle interaction effects and maximum heat generation for hyperthermia[12–15]. Curiously, most LRT studies from the literature do not dis-

cuss a fundamental limitation of the model, namely, that it is only valid at the low particle size range and low field amplitudes.

In Fig.1 we show the range of validity of the LRT, which, as can be seen, is far below the typical fields used for hyperthermia studies. There are several suggestions for identifying this limit. For example, Carrey et al.[16] found that the hysteresis area for a longitudinal case (field applied parallel to the easy axis - see Fig. 5(g) of Ref. [16]) deviates from the LRT for $\xi \leq 0.2$ ($\xi = \mu_0 M_S V H / k_B T$ - where M_S is the saturation magnetization, k_B is the Boltzmann constant and T is the temperature), which suggests that this model can only be applied for particles below a critical size. Alternatively, Verde et al. suggested that deviations occurs for fields $H < 0.02 H_K$ (H_K is the anisotropy field, that for uniaxial case is $H_K = 2K / \mu_0 M_S$ with K the anisotropy constant)[17, 18]. It is important to emphasize that experimentally, it is possible to determine if one is still in the linear regime or not, by verifying if the heating efficiency (also known as specific loss power - SLP) scales quadratically with the field. Throughout this manuscript, when discussing the theoretical models, low magnetic fields mean values within the LRT range. In addition, in Fig. 1 we also include an estimation of the range of validity of the nonlinear response model (NLRT) developed in this work, which will be shown later in the manuscript to be $H < 0.14 H_K$. This corresponds to a 7-fold increase in the range of field validity in comparison to the LRT definition used above. The result suggests that the model may be useful for biomedical applications, in particular for magnetic hyperthermia.

In the subject of heat loss, the term “nonlinear” has been used in a variety of ways. For instance, nonlinear dielectric effects have been related to the correlation of distinct relaxation times[19]. In this case, a superposition of Debye processes is used, which predict heat loss scaling with the square of field amplitude. Conversely, for relaxor ferroelectric materials a nonlinear polarization term is included in the dynamic response equation[20]. Such approach allowed the authors to investigate the third harmonics of the relaxor. On the other hand, in magnetic materials, nonlinear response is investigated using the stochastic Landau-Lifshitz-Gilbert (SLLG) equation[17, 18, 21, 22]. In this case, thermal fluctuations are addressed using the Brown’s approach[23], where the giant spin hypothesis allow one to use the Fokker-Planck equation to the magnetic moment orientational distribution function. One can then show that this leads to an infinite hierarchy of equations, which can be solved numerically to find the magnetic moment response of the nanoparticle [24–27]. The method is valid for any field amplitude, but due to its mathematical complexity, it does not yield simple analytical expressions that could be useful in the applied field.

Indeed, the field and frequency-dependence of heat loss in magnetic materials have been attracting the attention for a long time due to technological applications [28]. In general, the loss in magnetic materials can show several contributions, spanning from eddy currents (that scales with $f^2 H^2$), anomalous eddy current contributions (due to complex domain wall dynamics which scales with $f^{3/2} H^{3/2}$) up to multidomain magnetichysteresis contribution. The later term can be explained using the Rayleigh correction to the magnetic permeability and reveals a power loss scaling with $f H^3$. Curiously, this type of behavior had been reported before in magnetic nanoparticle hyperthermia experiments [29]. The authors suggest that this can be explained by the existence of large particles in the sample [29]. So, multidomain particles could be relevant to heat generation through domain wall motion loss. However, for most used magnetic fluid samples, multidomain particles are not expected. For example, in magnetite nanoparticles the single-domain limit is around 80 nm [30]. Moreover, on the theoretical point of view, Carrey et al. investigated the SLP field exponent using numerical simulations of the SLLG equation (see Fig. 7 of Ref. [16]). The authors found theoretically that this exponent is size dependent and showed values below or higher than 2. This type of behavior was found experimentally by Verde et al. [17]. However, in both works, no simple analytical expression was used to explain this behavior.

Here we show that through a modification of Bloch’s equation, which is linear with respect to the magnetization, one is able to obtain a heat loss expression valid beyond the LRT. Indeed, different from other works from the literature, we demonstrate that even the linear frequency term has higher order field contributions. Also, our model introduces a nonlinear frequency term which adequately describes the magnetic response within the hyperthermia therapeutic window. The validity of the model is explicitly tested by comparing it with numerical simulations of the SLLG approach. In addition, we included experimental magnetic hyperthermia data that supports our theoretical findings. Twelve powder samples were studied, including cobalt-ferrite, copper-ferrite, nickel-ferrite, maghemite and manganese-ferrite (doped with Zn or Co and also undoped) based nanoparticles. The analytical nonlinear response model is believed to be useful not only for improving our understanding of magnetic losses, but also may impact other related areas, which could benefit from analytical expressions, as for example, magnetic particle imaging[31, 32] and magnetic nanothermometry[33, 34].

The article is organized as follows: In section II we discuss several models from the literature. In particular, we present the linear response theory (LRT), the nonlinear Ferguson-Krishnan model (FK) (usually applied in magnetic particle imaging), the perturbation method developed by Raikher and Stepanov (RS model), and finally

the stochastic Landau-Lifshitz-Gilbert model, which is expected to be the exact solution of the magnetic response of the nanoparticle at alternating field conditions. All the models are critically compared showing the necessity of developing a simple nonlinear analytical model. The SLLG model is then compared with the proposed nonlinear response model (NLRT) developed in section III. Section IV we present the experimental procedure, i.e. the synthesis and characterization of magnetic fluids. In section V we discuss all the theoretical and experimental results. Here we focus on magnetic nanoparticle hyperthermia, but also compare our model with the third-harmonic magnetic particle imaging data from the literature. Finally, in section VI we summarize our findings.

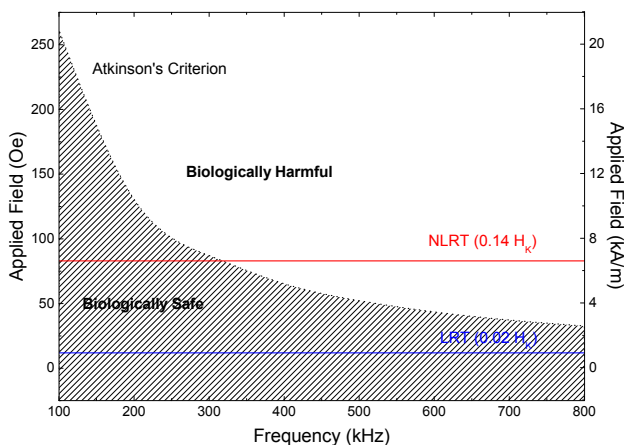


Figure 1. (Color online) The figure shows the calculated biological critical field according to Atkinson's criteria scaled for a coil radius of 0.035 m (expected for small tumors in breast [10]), which results in a $Hf < 20.78 \times 10^5$ kA/(m \times s). Human treatment can only occur below this field. The LRT limit is calculated assuming $H < 0.02H_K$ for a particle diameter of 15 nm, $M_S = 270$ emu/cm³, $K_{ef} = 8 \times 10^4$ erg/cm³, $T = 300$ K, $\alpha = 0.05$ and $\rho = 5$ g/cm³. The nonlinear response critical field for our model (NLRT) corresponds to the solid line.

II. MODELS REVIEW

All the models discussed in this manuscript are valid within the single-domain range. Also, they assume the giant-spin hypothesis of Brown[23], i.e. coherent spin rotation. Here we will consider the case of uniaxial magnetic nanoparticle, where the energy is given by

$$E = KV \sin^2 \theta - \mu_0 M_S V H \cos(\theta - \varphi). \quad (2)$$

The first term is the uniaxial anisotropy energy, while the other is the Zeeman interaction. θ represents the angle between the magnetic moment of the nanoparticle

and the easy axis direction, while $\theta - \varphi$ corresponds to the angle between the magnetic dipole and the applied field. It is common to name the longitudinal case as $\varphi = 0$, which is the case where the field is applied in the anisotropy axis direction.

The simplest quasi-static magnetization model in the literature, named Langevin model, neglects the anisotropy term, which can only be done if the ratio of this anisotropy contribution to the thermal energy is very low. In this case the magnetization can be calculated from

$$\frac{M}{M_S} = \langle \cos \theta \rangle = \frac{\int_0^\pi \cos \theta e^{\xi \cos \theta} \sin \theta d\theta}{\int_0^\pi e^{\xi \cos \theta} \sin \theta d\theta} = L(\xi). \quad (3)$$

$L(\xi) = \coth(\xi) - 1/\xi$ is the Langevin function, whose series expansion to fifth order gives

$$M = M_S \left(\frac{\xi}{3} - \frac{\xi^3}{45} + \frac{2\xi^5}{945} - \dots \right) \quad (4)$$

$$= \chi_{LA,1} H + \chi_{LA,3} H^3 + \chi_{LA,5} H^5 + \dots$$

The first term is the initial (linear) susceptibility, the second the cubic, and there on.

A. Linear Response Theory

The first linear response model to describe heat loss was probably described by Debye in the context of rigid electric dipoles[12]. Here we focus in the magnetic case. Let us first start by assuming that a magnetic particle is subjected to a harmonic field $H(t) = \Re \{ H_0 e^{i\omega t} \} = H_0 \cos \omega t$, with the magnetic susceptibility $\chi = \chi' - i\chi''$, where χ' and χ'' corresponds to the real and imaginary linear susceptibility terms, respectively. So, the magnetization term can be written as $M(t) = \Re \{ \chi H(t) \} = H_0 (\chi' \cos \omega t + \chi'' \sin \omega t)$, where $\omega = 2\pi f$ with f the field frequency. Therefore, defining the heating efficiency (SLP) as the frequency times the hysteresis loss divided by the particle density (ρ) one finds

$$SLP = \frac{f}{\rho V_p} \oint_{\text{cycle}} \delta Q = -\frac{f}{\rho} \mu_0 \oint M dH \quad (5)$$

$$= \pi \frac{f}{\rho} \mu_0 H_0^2 \chi''.$$

This equation represents the heat loss of the magnetic material. So, one now needs an expression for the imaginary susceptibility term. If the projection of the magnetization, $M(t)$, in the field direction satisfies the Bloch equation, i.e. $\tau(dM/dt) + M = \chi H(t)$, where τ is the magnetization relaxation time, one can show the linear susceptibility term is $\chi = \chi_0 / (1 + i\omega\tau)$, revealing that

$$\chi'' = \chi_0 \frac{\omega\tau}{1 + (\omega\tau)^2}. \quad (6)$$

χ_0 is the equilibrium susceptibility, which within the Langevin model is equal to $\chi_{LA,1}$. However, depending on the model this term would be different. The relaxation of the magnetization for an uniaxial nanoparticle is $\tau = \tau_0 e^\sigma / \sigma^{1/2}$ with $\sigma = KV/k_B T$, that is valid when $\sigma \geq 2$ [35]. Here V is the particle volume, T is the temperature, k_B in Boltzmann's constant and K the magnetic anisotropy. $\tau_0 = \sqrt{\pi} M_S (1 + \alpha^2) / (\gamma_0 2K\alpha)$ (about $10^{-10} - 10^{-8}$ s), with γ_0 the electron gyromagnetic ratio and α the dimensionless damping factor. For the field applied in the anisotropy direction one finds for the relaxation in the limit of high anisotropy

$$\tau_h = \frac{2\tau_0 \left[(1-h) e^{-\sigma(1-h)^2} + (1+h) e^{-\sigma(1+h)^2} \right]^{-1}}{\sigma^{1/2}(1-h^2)}. \quad (7)$$

The field term h is given in reduced units, i.e. $h = H_0/H_K$. This expression returns to the later in the absence of an applied field. The first one to describe this heat loss for magnetic fluids was Rosensweig[14]. The model above predicts a loss proportional to the square of the applied field. However, this is only true experimentally at low field amplitudes as found in several cases dealing with magnetic nanoparticles [17, 18, 29]. Note that the same issue occurs in the electric case for dielectrics[19] or relaxor ferroelectrics[20]. In addition, the LRT model predicts elliptical magnetic hysteresis curves, which have been observed at low field amplitudes (less than 4 kA/m) by Eggeman et al. [36] and Tomitaka et al. [37]. However, this is not consistent with findings at higher field amplitudes, as for instance in magnetic particle imaging where a nonlinear response plays a crucial role [31, 32].

B. Ferguson-Krishnan Approach

In an attempt to include nonlinear phenomena in the description, Ferguson and Krishnan[38] proposed a generalization of linear magnetization, using the Langevin function:

$$M(t) = M_S \left(\frac{1}{1 + (\omega\tau)^2} L(\xi \cos(\omega t)) + \frac{\omega\tau}{1 + (\omega\tau)^2} L(\xi \sin(\omega t)) \right). \quad (8)$$

This approach assumes that the frequency response of higher field order (quasi-static) terms are the same as the linear dynamic susceptibility term and neglects the quasi-static contribution from the magnetic anisotropy energy term. This expression is usually used to obtain the n th-order harmonic magnetization, which represents an important quantity in magnetic particle imaging [31, 32]. The harmonic calculation will be discussed in detail in section III.

C. Raikher-Stepanov Perturbation Method

Using perturbation theory, Raikher and Stepanov[39], included the anisotropy term and showed that the magnetization could be written as $M(t) = \Re(\chi_1 H_0 e^{i\omega t} + \chi_3 H_0^3 e^{3i\omega t} + \dots)$. However, different from the FK model above, the frequency dependence of the cubic term was found to be different from the linear term. The authors found that the cubic susceptibility could be written as

$$\chi_3 = -\frac{1}{4} \chi_3^{(0)} \frac{(1 + S_2^2)(1 - i\omega\tau)}{45(1 + i\omega\tau)(1 + 3i\omega\tau)}, \quad (9)$$

where $\chi_3^{(0)} = \phi \mu_0^3 M_S^4 V^3 / (k_B T)^3$, ϕ is the particle volume fraction of the assembly and $S_2 = \frac{1}{2} \int_0^1 (3x^2 - 1) \exp(\sigma x^2) dx / \int_0^1 \exp(\sigma x^2) dx$. So, the real and imaginary susceptibility terms are given by

$$\chi_3' = \frac{1}{180} \chi_3^{(0)} \frac{(1 + S_2^2)(7\omega^2\tau^2 - 1)}{(1 + \omega^2\tau^2)(1 + 9\omega^2\tau^2)}, \quad (10)$$

$$\chi_3'' = -\frac{1}{180} \chi_3^{(0)} \frac{(1 + S_2^2)\omega\tau(3\omega^2\tau^2 - 5)}{(1 + \omega^2\tau^2)(1 + 9\omega^2\tau^2)}. \quad (11)$$

Using up to the cubic term the magnetization of the nanoparticle in the RS model gives

$$M(t) = (\chi_1' \cos(\omega t) + \chi_1'' \sin(\omega t)) H_0 + (\chi_3' \cos(3\omega t) + \chi_3'' \sin(3\omega t)) H_0^3, \quad (12)$$

where $\chi_1' = \chi_1^{(0)}(1 + 2S_2)/(1 + (\omega\tau)^2)$, $\chi_1'' = \omega\tau\chi_1^{(0)}(1 + 2S_2)/(1 + (\omega\tau)^2)$, with $\chi_1^{(0)} = \phi \mu_0 M_S^2 V / (k_B T)$ and χ_3' and χ_3'' are given by Eq. 10 and Eq. 11. Note that those expressions are valid for an ensemble and low field amplitudes. In order to obtain the equivalent expressions for the nanoparticle one only need to neglect the particle volume fraction in the equilibrium susceptibilities. Because of the perturbation approach this model is expected to be valid only at very low field amplitudes.

D. Stochastic Landau-Lifshitz-Gilbert Model

The model that is expected to correctly describe the magnetization response of a single-domain nanoparticle at any field amplitude and frequency range is the SLLG model. In this case, the magnetic moment of the nanoparticle is assumed to be described by the Landau-Lifshitz-Gilbert equation

$$\frac{d\vec{M}}{dt} = -\gamma \vec{M} \times \vec{H}_{\text{eff}} - \frac{\alpha\gamma}{M_S} \vec{M} \times (\vec{M} \times \vec{H}_{\text{eff}}), \quad (13)$$

where

$$\vec{H}_{\text{eff}}(t) = \vec{H}(t) + \vec{H}_{\text{ani}} + \vec{H}_{\text{th}}(t). \quad (14)$$

The effective field has three contributions: the applied external field, the anisotropy field and the thermal fluctuation field. So the Landau-Lifshitz-Gilbert equation for a magnetic dipole is augmented with a Gaussian white noise thermal field \vec{H}_{th} whose Cartesian coordinates satisfy the statistical properties: $\langle \vec{H}_{\text{th}}^i(t) \rangle = 0$ and $\langle \vec{H}_{\text{th}}^i(t) \vec{H}_{\text{th}}^j(s) \rangle = 2(k_B T \alpha / V) \delta_{ij} \delta(t-s)$. The Kronecker and Dirac deltas indicates that the thermal field is both spatial and temporally uncorrelated. In principle, one could use the equation above and do numerical simulations. However, the approach of Brown was to connect the SLLG equation to the Fokker-Planck equation of the magnetic moment orientational distribution function [23], which can be used to obtain the nanoparticle magnetic moment response.

In this work we focus in the longitudinal case. The first authors to study in detail this problem analytically was Dejardin and Kamilkov [24]. Later, others used the same approach to describe dynamic magnetic hysteresis [25–27]. Here, the magnetic moment orientational distribution function $f(z, t)$ can be shown to obey the Fokker-Planck equation

$$2\tau_N \frac{\partial f}{\partial t} = \frac{\partial}{\partial z} \left[(1 - z^2) \left(\frac{\partial f}{\partial z} - f(z, t) h_{\text{eff}}(z, t) \right) \right], \quad (15)$$

with $\tau_N = \frac{\mu(1 + \alpha^2)}{2\gamma_0 \alpha k_B T}$ the free diffusion time, $z = \cos \theta$ and θ the angle between the magnetic dipole and the applied field. The magnetic anisotropy is assumed uniaxial. So, the ratio of the particle energy to thermal energy can be written as

$$\frac{U_{\text{eff}}}{k_B T} = -\sigma z^2 - 2h\sigma z, \quad (16)$$

where the field term $h = H/H_K$. Therefore, the effective field is

$$h_{\text{eff}} = -\frac{1}{k_B T} \frac{\partial U_{\text{eff}}}{\partial z} = 2\sigma(h + z). \quad (17)$$

The Fokker-Planck equation is then used to obtain the time evolution of the l th-order moment $p_l(t) = \langle P_l \rangle$, which is shown to be described by

$$2\tau_N \frac{dp_l}{dt} = \frac{l(l+1)}{2l+1} (A_1 + A_2) - l(l+1)p_l, \quad (18)$$

with

$$A_1 = 2\sigma h(p_{l-1} + p_{l+1}), \quad (19)$$

and

$$A_2 = 2\sigma \left[\frac{l-1}{2l-1} p_{l-2} + \frac{2l+1}{(2l-1)(2l+3)} p_l - \frac{l+2}{2l+3} p_{l+2} \right]. \quad (20)$$

This equation shows that each moment depends on others in a nonlinear fashion. This infinite hierarchy may be solved numerically using fast sparse solvers [17, 22, 25, 27] and discarding several periods of the external field. Alternatively, one could also expand the $p_l(t)$ in a Fourier series as

$$p_l(t) = \sum_{k=-\infty}^{\infty} F_k^l(\omega) e^{ik\omega t}, \quad (21)$$

with all $p_l(t)$ real, which implies that $F_{-k}^l = (F_k^l)^*$, where the asterisks refer to the complex conjugate [24]. This will then lead to a hierarchy of algebraic equations for the Fourier amplitudes, which also need to be solved numerically [24].

E. Magnetization Loops

We are now in condition to compare the hysteresis loops of each model, namely the linear response theory using the field-independent relaxation time (LRT) and also the field-dependent relaxation time of Eq. (7) (LRT τ_h), the FK model, the RS model and the exact solution for the SLLG model. In Fig. 2(a) we show the magnetization curves of all those models. It is clear that the LRT model, independent of the relaxation time equation used, shows an elliptical loop. The RS model showed a similar behavior. The only model that shows a significant difference from LRT is the FK model. However, it also shows an elliptical hysteresis, which is distinct from the LRT model because of the Langevin equilibrium susceptibility. So, different from the other models, it does not take into account the anisotropy term. Nevertheless, for the parameters used in this simulation, it is shown that none of the models above represent well the exact solution given by the SLLG magnetization hysteresis loop. Although improvements were obtained in each model, in general they are not yet satisfactory. Motivated by this fact, we decided to work out a nonlinear response model, from now on named NLRT model. This model is able to better represent the magnetization response at higher field conditions, not only in comparison to the LRT, but also far better than the FK or RS models.

III. THEORETICAL MODEL

In this section we present our nonlinear response model. Firstly, we include the magnetic anisotropy energy term in the longitudinal case, which allow us to obtain any quasi-static (equilibrium) susceptibility terms. Those expressions will be named $\chi_{QS,n}$, i.e. the n th-order quasi-static (QS) coefficient obtained in the low-frequency limit ($\omega \rightarrow 0$). In the next subsection we introduce our dynamic model, where a new expression for

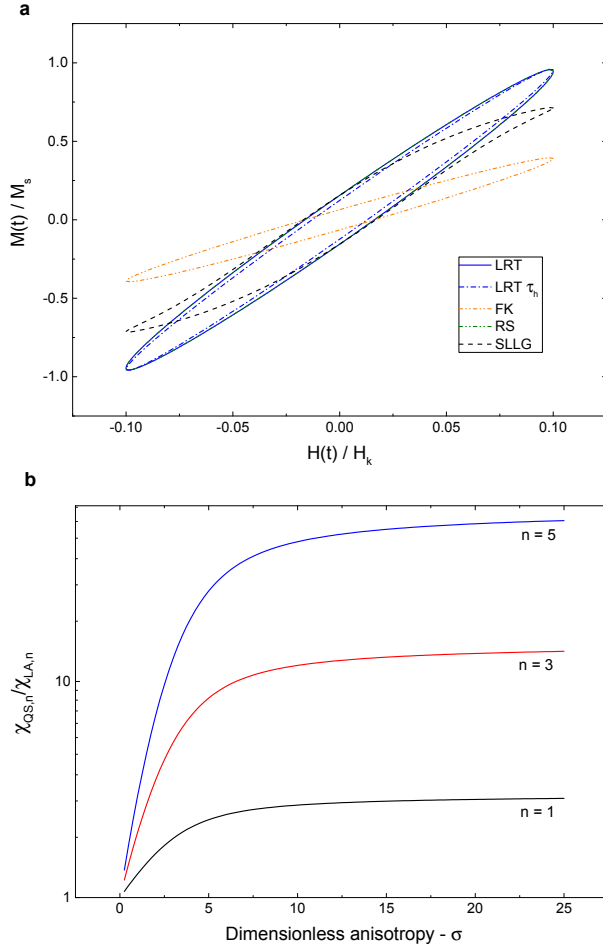


Figure 2. (Color online) (a) Dynamic hysteresis curves for the LRT, LRT considering field dependence on relaxation time τ , Ferguson-Krishnan approach, Raikher Stepanov method and numerical solution of SLLG for $\sigma = 6$ and $\omega\tau_0 = 10^{-3}$. (b) Longitudinal to Langevin susceptibilities ratio for $n = 1$, $n = 3$ and $n = 5$.

the heat loss and the particle magnetization is obtained. The last subsection is related to the cubic harmonic calculation, which is an important parameter for magnetic particle imaging application.

A. Quasi-static longitudinal case

For an uniaxial magnetic nanoparticle in the longitudinal case, the average magnetization is obtained from

$$\frac{M}{M_S} = \langle \cos \theta \rangle = \frac{\int_0^\pi \cos \theta e^{\sigma \cos^2 \theta + \xi \cos \theta} \sin \theta d\theta}{\int_0^\pi e^{\sigma \cos^2 \theta + \xi \cos \theta} \sin \theta d\theta}. \quad (22)$$

For $\sigma > 0$, one can show that the longitudinal magnetization is [40]

$$M = M_S \left(\frac{2i \sinh(\xi)}{\sqrt{\sigma\pi}} \frac{e^{\sigma + \frac{\xi^2}{4\sigma}}}{\operatorname{erf}\left[i\left(\sqrt{\sigma} + \frac{\xi}{2\sqrt{\sigma}}\right)\right] + \operatorname{erf}\left[i\left(\sqrt{\sigma} - \frac{\xi}{2\sqrt{\sigma}}\right)\right]} - \frac{\xi}{2\sigma} \right). \quad (23)$$

Expanding the longitudinal magnetization in a Taylor series:

$$\begin{aligned} M &= M_S \left[\frac{ie^\sigma}{\sqrt{\sigma\pi}\operatorname{erf}(i\sqrt{\sigma})} - \frac{1}{2\sigma} \right] \xi + M_S \left[\frac{e^\sigma (6\sigma e^\sigma + i\sqrt{\sigma\pi}(2\sigma + 3)\operatorname{erf}(i\sqrt{\sigma}))}{12\pi(\sigma\operatorname{erf}(i\sqrt{\pi}))^2} \right] \xi^3 + \dots \\ &= \chi_{QS,1}H + \chi_{QS,3}H^3 + \dots, \end{aligned} \quad (24)$$

where $\operatorname{erf}(iz) = (2i/\sqrt{\pi}) \int_0^z e^{-u^2} du$ and $\chi_{QS,3} < 0$. Note that all $\chi_{QS,n}$ are real. In Fig. 2(b) we show the ratio of the $\chi_{QS,n}/\chi_{LA,n}$ up to the fifth-order ($n=5$).

The longitudinal linear susceptibility ($\chi_{QS,1}$) calculation demonstrate that in the absence of (or very low) magnetic anisotropy the susceptibility approaches the ex-

pected Langevin result. On the other hand, in the high anisotropy limit, the linear ratio approaches 3, which indicates that the longitudinal result tends to the Ising result, as expected in this case. Other ratios are also shown in the figure. Therefore, we can conclude that in general it is of great importance to include the anisotropy term when investigating the magnetic response of nanoparticles.

B. Nonlinear Response Model

As in LRT model, let us assume that a magnetic particle is subjected to a harmonic field and that the projection of the magnetization, $M(t)$, in the field direction satisfies the Bloch equation, i.e.

$$\tau \left(\frac{dM}{dt} \right) + M = f(t), \quad (25)$$

where τ is the relaxation time and $f(t)$ is a function of the alternating field. Hence, it will be periodic, i.e. $f(t) = f(t + 2\pi/\omega)$. Also, in general one might represent $f(t) = \chi_1 H(t) + \chi_3 H(t)^3 + \dots$, where χ_n is the n th-order magnetic susceptibility. The LRT, discussed before, corresponds to considering just the first term in $f(t)$. The nonlinear response under Bloch's assumption may be computed as follows. In general $f(t)$ is a function of $H(t)$ so it may be expanded in a cosine series as $f(t) = \sum_{n=1}^{\infty} c_n \cos(n\omega t)$ for certain coefficients c_n , that can be easily identified by expanding $f(t)$ in terms of $\cos(n\omega t)$ (another alternative way to obtain those coefficients is using the integrating factor method directly to Bloch's equation). The steady-state solution of the Bloch equation is therefore

$$M(t) = \sum_{n=1}^{\infty} c_n \frac{\cos n\omega t + (n\omega\tau) \sin n\omega t}{1 + (n\omega\tau)^2}. \quad (26)$$

In this approach, the corresponding SLP is

$$\begin{aligned} \text{SLP} &= \frac{\pi f}{\rho} H_0 \frac{\omega\tau}{1 + (\omega\tau)^2} c_1 \\ &= \frac{\pi f}{\rho} \frac{\omega\tau}{1 + (\omega\tau)^2} \left(\chi_1 H_0^2 + \frac{3}{4} \chi_3 H_0^4 + \frac{5}{8} \chi_5 H_0^6 + \dots \right). \end{aligned} \quad (27)$$

This means that one only needs to worry with the coefficient $c_1(H_0)$. This comes from the fact that in the heat loss integral only the terms obtained from $n = 1$ is nonzero. Note that the first term corresponds to the usual Debye model, if one assumes that $\chi_1 = \chi_{QS,1}$, i.e. that χ_1 is the quasi-static limit linear coefficient. Also, it might be important to mention that the existence of the higher order field dependent terms indicate a correction not reported before in the literature. As for instance, if one uses the magnetization equation of the RS model, only the the quadratic field term appears. The same approach can also be used in the dielectric loss case. For

example, the electric field dependence dielectric loss of glycerol (see inset of Fig. 3 of Ref [19]).

According to equation (26), the Bloch solution for the magnetization $M(t)$ up to cubic terms in the field is

$$\begin{aligned} M(t) &= \left(\chi_1 H_0 + \frac{3}{4} \chi_3 H_0^3 \right) \frac{\cos(\omega t) + \omega\tau \sin(\omega t)}{1 + (\omega\tau)^2} \\ &+ \frac{\chi_3 H_0^3}{4} \frac{\cos(3\omega t) + 3\omega\tau \sin(3\omega t)}{1 + (3\omega\tau)^2}, \end{aligned} \quad (28)$$

where χ_n are the n th-order magnetic susceptibility coefficients. In the equation above is clear that higher-order terms are also relevant to the magnetization dynamics. As for instance, this nonlinearity effect can be identified even for the first harmonic contribution, which shows higher field order terms.

In addition, if $\omega\tau \ll 1$ one may write the magnetization (considering higher-order terms in $f(t)$) as $M(t) = \chi_1 H_0 \cos(\omega t) + \chi_3 H_0^3 \cos(\omega t)^3 + \dots$. For the sake of argument, if one assumes that the n th-order susceptibility terms are equal to the quasi-static terms ($\omega \rightarrow 0$) and that the nanoparticle is at the superparamagnetic regime, than $M(t)/M_S = L(\xi \cos(\omega t)) + \mathcal{O}(\omega\tau)$. Note that the first term of this equation has been used systematically in both, magnetic particle imaging (MPI)[31] and magnetic nanothermometry (MNT)[33, 34]. In MNT the magnetization expression was shown to be useful only at the low frequency range[33], which is easily explained by our model due to the range of validity of the later expression. Moreover, in MPI the magnetization is similar, but not identical to our model, and differs mainly due to the term $n\omega\tau$ and that the later assumes quasi-static susceptibility terms and superparamagnetic particle. As a consequence, our model give different higher-order harmonic magnetization terms and might represent better the experimental MPI data[38]. Curiously, our model gives a similar expression as Ref. [38] for the heat loss if we assume that $\chi_n = \chi_{QS,n}$. However, this approximation does not represent correctly the magnetization dynamics.

Further, Eq. (27) shows that the Bloch equation predicts the same frequency dependence as the LRT, which will result in elliptical-like hysteresis curves that are in disagreement with experiment. The reason for this discrepancy is that Bloch's equation is linear, whereas the underlying physical phenomena is not, as discussed before in section II-D. One way to circumvent this is to assume that the coefficients χ_n depend explicitly on ω . The exact form of this dependence is problem specific, but it must be such that when $\omega \rightarrow 0$, one recovers the equilibrium nonlinear susceptibilities. The heuristic improvement approach, also used by others[39], is able to better represent the magnetization dynamics.

So, to correct for the aforementioned deficiency of the Bloch approach, we replace χ_n with a frequency dependent function and compare the approximation with exact

results, which are obtained for the longitudinal case using the SLLG model[17, 18, 22, 35]. In this strategy we wrote $\chi_n = \chi_{QS,n}g_n$, where g_n is a function of the frequency. The quasi-static susceptibility coefficients were obtained from the series expansion of the quasi-static longitudinal solution[40]. Also, from our assumption is obvious that one should have $g_n(\omega\tau \rightarrow 0) = 1$. Moreover, for the first term we should have $g_1 = 1$, which corresponds to the LRT result. For the cubic term we found that

$$\chi_3 = \chi_{QS,3} \frac{3 - (\omega\tau)^2}{3(1 + (\omega\tau)^2)}. \quad (29)$$

Similarly as the RS model, the magnetization can be written in the same functional form as Eq. (12). However, now the real susceptibility terms are

$$\chi'_1 = \frac{\chi_{QS,1}}{1 + (\omega\tau)^2} + \frac{1}{4}H_0^2\chi_{QS,3} \frac{3 - (\omega\tau)^2}{(1 + (\omega\tau)^2)^2}, \quad (30)$$

$$\chi'_3 = \frac{1}{12}\chi_{QS,3} \frac{3 - (\omega\tau)^2}{(1 + (\omega\tau)^2)(1 + (3\omega\tau)^2)}, \quad (31)$$

while the imaginary terms are $\chi''_1 = \omega\tau\chi'_1$ and $\chi''_3 = 3\omega\tau\chi'_3$. Those results indicate that the susceptibility terms are distinct from the RS model (see Eqs. 10 and 11), even though the quasi-static susceptibility coefficients give the same result. Also, the linear susceptibility term shows a nonlinear field and frequency contribution, which was absent in other models.

So, returning to the heat loss integral (Eq. (5)) and using the cubic magnetization (Eq. (28)) with this correction (Eq. (29)), the new expression for SLP is now given by

$$SLP = \mu_0\pi \frac{f}{\rho} H_0^2 \left[\frac{\chi_{QS,1}\omega\tau}{1 + (\omega\tau)^2} + \frac{1}{4}H_0^2\chi_{QS,3}\omega\tau \frac{(3 - (\omega\tau)^2)}{(1 + (\omega\tau)^2)^2} \right]. \quad (32)$$

Moreover, in section V, besides discussing the magnetic nanoparticle hyperthermia, the cubic harmonic magnetic particle imaging (MPI) experimental signal data obtained in Ref. [38] will also be compared with the theoretical calculations using the FK model and the NLRT model (see section V for details). We will show a better agreement with experimental data using the nonlinear response theoretical model developed in this work. In addition, because we also investigate soft-magnetic nanomaterials (low σ), the empirical uniaxial relaxation time expression, valid for any anisotropy value, has been considered [35]

$$\tau = \tau_0 (e^\sigma - 1) \left[2^{-\sigma} + \frac{2\sigma^{3/2}}{\sqrt{\pi}(1 + \sigma)} \right]^{-1}. \quad (33)$$

IV. EXPERIMENTAL PROCEDURE

Manganese-ferrite samples were synthesized by hydrothermal route and separated for the hyperthermia analysis after characterization by x-ray diffraction (XRD) and vibrating sample magnetometer (VSM). All chemical reagents (FeCl₃.6H₂O, MnCl₂.4H₂O, ZnCl₂, CoCl₂.6H₂O) citric acid trisodium salt - Na₃C₆H₅O₇, methylamine - CH₃NH₂, and acetone - CH₃COCH₃) were purchased with analytical quality and used without any further purification. In a typical approach, Mn_{0.75}[(Zn or Co)]_{0.25}Fe₂O₄ magnetic nanoparticles were prepared as follows: adequate amounts of 1.0 mol/L metal stock solutions were diluted with 40.0 mL of distilled water to form a precursor solution containing 10.0 mmol of Fe³⁺, 3.75 mmol of Mn²⁺, and 1.25 mmol of Zn²⁺ or Co²⁺. Thus, 120 mmol of methylamine at 40% (w/w) were quickly poured into the stock solution under vigorous stirring for 10 min and then transferred into a 120 mL Teflon-sealed autoclave and heated up to 160°C for 6 h. After cooling to room temperature, the precipitate was separated by magnetic decantation, washed with H₂O three times and re-dispersed in 50.0 mL of water. Then, 4.0 mmol of citric acid trisodium salt was added into the solution which was heated up to 80°C for 60 min. After adjusting the pH of slurry to 7.0 and washing with acetone three times, the precipitate was re-dispersed in 50.0 mL of water to form a magnetic sol, after evaporating residual acetone. Thus, a size-sorting process was done by adding 1 g of NaCl to the as-prepared magnetic sol[41]. 5 min afterwards under a permanent magnet (NdFeB), salt adding induced a phase transition and formed an upper (bottom) sol phase with populations of smaller (larger) nanoparticles. Once separated, precipitate of each phase was washed twice with a mixture water/acetone 1:10 (volume/volume) and, after evaporating residual acetone, nanoparticles were re-dispersed in water. This procedure was repeated several times. Powders were obtained from evaporation of sols at 55°C for 8 h. Details about cobalt-ferrite samples can be found in Ref. [18] and copper-ferrite and nickel-ferrite samples can be found in Ref. [17].

After the size-sorting process powder samples were analyzed by XRD (Shimadzu 6000) to separate samples with similar sizes. The previous analysis was performed using the well-known Scherrer equation, which is given by $D_{XRD} = \kappa\lambda/\beta \cos \psi$, where $\kappa = 0.89$ is the Scherrer constant, $\lambda = 0.15406$ nm is the X-ray wavelength, β is the line broadening in radians obtained from the square root of the difference between the square of the experimental width of the most intense peak to the square of silicon width (calibration material), and ψ is the Bragg angle of the most intense peak (311). This procedure allowed us to select three distinct samples of similar sizes containing MnFe₂O₄, Mn_{0.75}Zn_{0.25}Fe₂O₄, or Mn_{0.75}Co_{0.25}Fe₂O₄

nanoparticles. All the nanoparticles were surface-coated with citric acid, which guarantee stability at physiological conditions. The samples were also characterized by VSM (ADE Magnetics, model EV9, room temperature measurements, field up to 2T). Table I summarizes the relevant characterization properties of the nanoparticles.

Finally, magnetic hyperthermia data was obtained in two systems, one home-made which operates at 500kHz, and another one from nanoTherics. In particular, the later system operates in a broad frequency range, spanning from 110 up to 980kHz. While details about the home-made hyperthermia system has been described elsewhere [17, 18]. The calorimetric method used to obtain the experimental SLP of the sample used the equation

$$SLP = \frac{C}{m_{NP}} \left[\frac{dT}{dt} \right]_{max}, \quad (34)$$

where C is the heat capacity of the sample (here assumed as the heat capacity of the liquid carrier due to the low concentration of particles), m_{NP} is the mass of magnetic nanoparticles in unit of grams (obtained from the analysis of the magnetisation curves of the colloid samples), T is the temperature of the sample measured with a fibre optic thermometer. Note that in the SLP calculation we use the value of the maximum rate of temperature increase ($[dT/dt]_{max}$), as discussed previously by others [17, 42]. This method is believed to better estimate SLP than the most common initial-slope procedure that can underestimate this value [43].

V. RESULTS AND DISCUSSION

A. Theoretical results

Several experimental results show the existence of an optimal particle size for hyperthermia [16, 18, 30]. This is also contemplated in Eq. (6), which predicts that this optimal size should occur when $\omega\tau = 1$. This, however, is only true at low field amplitudes. Increasing field amplitude one notice a shift of maximum size towards larger particles in a noninteracting system. This can be easily modelled within LRT using the field dependent magnetization relaxation time [24]. Indeed, such drift becomes clear when $h > 0.04$ (see discussion of Fig. 3(f) below). Further, numerical dynamic hysteresis simulations using the SLLG model or Kinetic Monte Carlo method [16–18, 44] show that, as the field amplitude increases, the optimal size shifts towards larger particles. It may even disappear, depending (also) on the magnetic anisotropy of the nanoparticle [16–18, 44]. Most of the results above consider a noninteracting system. However, in colloids, or real in vivo situation, agglomerate formation plays a key role. In this case, it has been shown within LRT, that the opposite effect occurs, i.e. increasing the strength of

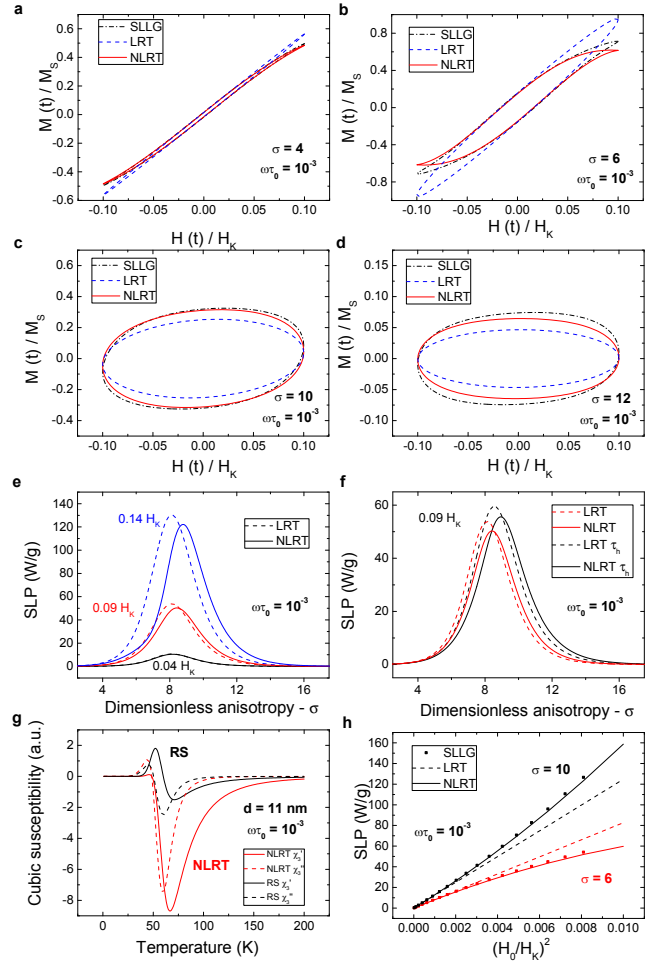


Figure 3. (Color online) Dynamic hysteresis curves for the LRT (dashed line), NLRT (solid line) and the exact solution (dash-dot line) using the SLLG equation for field $H_0 = 0.1H_K$ and $\omega\tau_0 = 10^{-3}$. In (a) $\sigma = 4$, (b) $\sigma = 6$, (c) $\sigma = 10$ and (d) $\sigma = 12$. (e) SLP as function of σ for the LRT and NLRT with distinct field amplitudes. (f) SLP as function of σ for the LRT and NLRT with and without the field dependence on the relaxation time. (g) Real and imaginary susceptibilities as function of temperature for the RS and the NLRT models. (h) SLP as a function the square of the field for the LRT (dash), NLRT (solid) and exact solution using the SLLG (points) for σ values of 6 and 10.

particle interaction shift the optimal diameter to lower sizes [15]. The same was found including particle-particle interaction using a mean field approach to the SLLG model at the low field regime [27]. Anyway, a valuable analytical nonlinear response theoretical model (NLRT) should be able to explain at least some of the features discussed above.

A comparison between the hysteresis curves obtained from the LRT, our NLRT model and the numerical solution of the SLLG model is shown in Fig.3(a)-(d), for distinct σ values considering $\omega\tau_0 = 10^{-3}$ and $H_0/H_K = 0.1$. It is found that the inclusion of the corrected cubic term

leads to a good agreement with the numerical simulations, adequately describing the deviations from the linear response. Note that the agreement is far better than any other model discussed previously (see Fig. 2(a)). The LRT model is shown as a dash line, the exact result using the SLLG equation is shown as dash-dot line, while NLRT (considering Eq. (29)) is shown as solid line. It is very surprising that, with such a simple assumption, an interesting nonlinear effect is obtained able to represent far better the magnetization dynamics. Indeed, we found that the present model works very well close to this limit of anisotropy value ($H_0 \cong 0.14H_K$). It also has a slight frequency dependence which can be monitored by non-physical results in the magnetization curve or kinks in the SLP versus σ curves increasing the field. At higher fields we observe deviations from the exact solution that might be only addressed if higher-order terms are determined. Nevertheless, as shown in Fig. 1 (see the NLRT line), the range of validity of the model is almost completely within the hyperthermia therapeutic window. This suggests that this model might be applicable for real clinical situations.

Figure 3(e) shows the SLP as function of σ for the LRT (dashed line) and the NLRT (solid line) for distinct field amplitudes. For simplicity, we are not considering the field dependence on the relaxation time. One can clearly observe a shift of the maximum of SLP towards higher particle sizes in the nonlinear case. Also a decrease of the maximum SLP value for the NLRT case. The phenomenon is strictly related to the nonlinear effect introduced in the model and not due to the field effect from the relaxation. This result is in accordance with numerical simulations from the literature [18, 44]. On the other hand, Fig. 3(f) also shows SLP as function of σ in both cases, but now investigating the field effect on the relaxation time for $H = 0.09H_K$. Similar behavior as before is observed. Nevertheless, in comparison with the LRT, the NLRT- $\tau(H)$ shows a larger size shift. As for instance, the optimum anisotropy term change from $\sigma_{opt} = 8.1$ for LRT to $\sigma_{opt} = 9.0$ for NLRT- $\tau(H)$, which corresponds to a shift in optimal diameter of the order of 4%.

As discussed in section II, there are other nonlinear models. In particular, cubic susceptibility expressions using the RS model had been suggested to represent experimental data of noninteracting magnetic nanoparticles [45]. Figure 3(g) shows the cubic susceptibility terms, imaginary and real, for the RS model and the NLRT model as a function of temperature. Here the parameters used were $d = 11$ nm, $M_S = 270$ emu/cm³, $K_{ef} = 8 \times 10^4$ erg/cm³, $\alpha = 0.05$ and $\rho = 5$ g/cm³. As found in Ref. [39] the real cubic term in the RS model shows a significant variation as a function of temperature, in particular in the range below 60 K, where a quite high positive cubic value is found theoretically. It is curious to notice that experimentally such effect has not been observed in Ref. [45] for noninteracting nanoparticle sam-

ples. In fact, discrepancies between the RS model and data of Ref. [45] had been attributed to polydispersity and particle-particle interaction effects. Note that the inclusion of such effects could be responsible for some of those differences between theory and data. However, there might be another explanation. As we have just shown, the NLRT model represents far better the magnetization response. Differently from the RS model, the real cubic susceptibility from NLRT does not show such strong positive contribution at low temperatures. As a consequence it might represent better experimental data. Another point that could be commented about the improvement in the NLRT model in comparison to others is the SLP calculation. Note that in the RS model the SLP calculation, using the magnetization expression of Eq. (12), provides the same result as the LRT. So, although the magnetization equations are not the same, the hysteresis area is the same as the LRT case. Again, this is in contradiction with several experimental results. From the experimental point of view, after obtaining the SLP data of the samples as a function of the applied alternating field, it is common to try to describe the heating efficiency in terms of a field exponent, i.e. one might try to fit the data with an allometric expression as $SLP = aH^\nu$, where a is a constant and ν the field exponent. If this exponent is equal to 2 one might argue that the sample is within the linear response regime.

Figure 3(h) shows the SLP as a function of the quadratic field for distinct σ values considering the LRT (dash), NLRT (solid) and SLLG (points). Both situations shows that depending on the particle size or anisotropy, deviations from the expected quadratic field dependence of the LRT are found. At the low barrier regime ($\sigma < \sigma_{opt}$), i.e. for particle sizes lower than the optimum value, the field dependence exponent is lower than 2. While at the high barrier regime, an exponent higher than 2 is observed. The same behavior is found from SLLG, as expected since NLRT model is based on the assumption that SLLG is the exact result. However, because in the NLRT only the cubic term was introduced, deviations between both models are expected for higher fields. The nonlinear regime has been studied experimentally before on Ref. [17], where the transition to the nonlinear regime was explained using the SLLG model, though without any analytical expression. The explanation for such behavior may be understood using Eq. (28). Note that $\chi_{QS,3} < 0$, so when $\omega\tau < \sqrt{3} \approx 1.7$ the high-order contribution term lowers the linear SLP field dependence term. The consequence of this is an apparent field exponent lower than 2. On the other hand, when $\omega\tau > \sqrt{3}$ the higher order SLP term changes sign, which now adds a value to the first order term. In this case exponents larger than 2 might appear if the field is high enough.

Sample	D_{XRD} (nm)	M_S (emu/cm ³)	H_{coer} (Oe)	ν
MnFe ₂ O ₄	11.3	293	21	2.2
Mn _{0.75} Zn _{0.25} Fe ₂ O ₄	11.1	302	0.4	1.6
Mn _{0.75} Co _{0.25} Fe ₂ O ₄	11.4	309	77	2.6
CoFe ₂ O ₄	9.1	272	152	3.9
γ -Fe ₂ O ₃	9.3	209	2.7	2.0
CuFe ₂ O ₄	9.4	124	0.5	1.2
CoFe ₂ O ₄	3.4	103	1.4	1.9
CoFe ₂ O ₄	12.9	253	261	2.5
CoFe ₂ O ₄	13.6	281	299	5.5
NiFe ₂ O ₄	5.3	153	0.3	1.5
NiFe ₂ O ₄	7.9	151	0.4	2.1
NiFe ₂ O ₄	12.8	185	4.4	2.3

Table I. Characterization parameters of the samples. D_{XRD} crystalline size, M_S saturation magnetization and H_{coer} coercive field. ν is the apparent SLP field exponent from allometric fit.

B. Magnetic hyperthermia evidence

Evidence of nonlinear behavior the SLP field dependence can be found in distinct ferrite-based powder samples. Table I summarizes the parameters obtained from sample analysis. Four sets of samples were studied. The first set is composed of three samples: manganese-ferrite based nanoparticles undoped, doped with zinc and doped with cobalt. Since samples were produced using the same method, have (approximately) the same magnetization, and the same diameter, this set allow the study of anisotropy influence over SLP versus H behavior. The second set is composed by other three samples: cobalt-ferrite, maghemite and copper-ferrite. These samples have very different magnetization and anisotropy, but the same diameter (some results published in Ref. [18]). The third set is composed by other three samples of cobalt-ferrite, which have a high anisotropy, with different diameters. And, the last set is composed by three samples of nickel-ferrite, which have a lower anisotropy than cobalt-ferrite, with different diameters.

Magnetic hyperthermia experimental data around 500 kHz is shown in Figs. 4(a), 4(c), 4(e) and 4(g) for powder samples, where we present the SLP as a function of the applied field for distinct ferrite-based samples. Most of the applied fields are above the therapeutical values (see Fig.1), but are necessary to experimentally observe deviations from LRT. Symbols represent experimental data, while the lines are the fit of the data using the allometric function. Firstly, notice that soft-like materials heat more efficiently at low field amplitudes, in agreement with what was found before experimentally and theoretically [15, 17, 18]. This property, although not discussed in this work, is relevant for in vivo applications

[5]. Table I shows the apparent field exponents obtained from this type of phenomenological approach for all the samples, as well Figs. 4(b), 4(d), 4(f) and 4(h), compared with 2 (gray dashed line which represents LRT). The result indicates deviation from linear behavior and the samples shows distinct exponents values, depending (probably) on sample anisotropy. The same behavior has been observed with other ferrites [17]. This behavior is in accordance with our previous theoretical analysis. However, a direct comparison between experimental data and theoretical analysis is compromised by the fact that sample are solid, allows a random anisotropy axis nanoparticle configuration that decreases the equilibrium susceptibility values lowering the SLP [17]. So, the nanoparticles at this highly packed configuration are at strong interacting conditions, which may affect the magnetic anisotropy [15, 17]. In this case, one can not use the longitudinal calculation developed in this work for the powder samples, since the quasi-static susceptibility values are now different. Nevertheless, powder configuration inhibit frictional loss contributions due to the Brownian relaxation mechanism [46–48] and a similar behavior for SLP (with distinct absolute values) is also expected.

The NLRT model developed here is valid for $H \leq 0.14H_K$, where magnetization relaxation mechanisms plays a role in the spin reorientation by overcoming the barrier energy. Increasing the field value one need to use directly the SLLG model, which due to the complexity of the problem does not reveal any simple analytical equation. Nevertheless, a simple approach for qualitative analysis under high field conditions ($H > H_K$) might be achieved using the Stoner-Wohlfarth (SW) model [13].

C. Magnetic particle imaging evidence

Besides magnetic hyperthermia, the present model might be useful for magnetic particle imaging (MPI) too. MPI is a nonionizing imaging technique, introduced in 2005 by Gleich and Weizenecker [31], which is capable of imaging magnetic tracers through the nonlinear magnetic response of magnetic nanoparticles. In MPI a DC plus an AC field are applied to the magnetic material in such a way to create a free field point volume where the nanoparticles can respond to the ac field excitation. The magnetic response signal can then be measured using detector coils. The received voltage by the detector coil is

$$u = -\mu_0 \int_V S_0(x) \frac{\partial M(x, t)}{\partial t} dV, \quad (35)$$

S_0 is the coil sensitivity (assumed to be $\mu_0 S_0 = 2.25$ mT/A) and the integration is over the magnetic material. The MPI third harmonic magnetization signal per unit volume $\mathbf{emf}_{3\omega_0}$ is defined as the module of

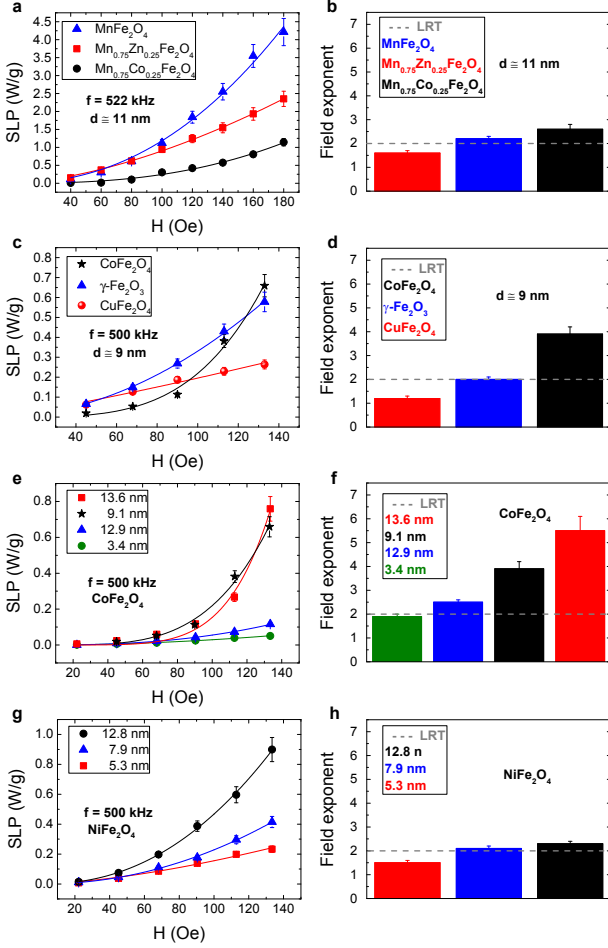


Figure 4. (Color online) (a) SLP as function of the magnetic field for distinct manganese-ferrite nanoparticles around 11 nm in powder configuration at $f = 522$ kHz. (b) Apparent SLP field exponent ν obtained for manganese-ferrite in powder configuration. (c) SLP as function of the magnetic field for distinct ferrite nanoparticles around 9 nm in powder configuration at $f = 500$ kHz. (d) Apparent SLP field exponent ν obtained for distinct ferrite nanoparticles in powder configuration. (e) SLP as function of the magnetic field for cobalt-ferrite nanoparticles with distinct sizes in powder configuration at $f = 500$ kHz. (f) Apparent SLP field exponent ν obtained for cobalt-ferrite in powder configuration. (g) SLP as function of the magnetic field for nickel-ferrite nanoparticles with distinct sizes in powder configuration at $f = 500$ kHz. (h) Apparent SLP field exponent ν obtained for nickel-ferrite in powder configuration. Symbols are data and lines represent the best fit using the allometric function.

the Discrete Fourier Transform given by

$$\mathbf{emf}_{3\omega_0} = \mu_0 S_0 |DFT[u_3]|, \quad (36)$$

where

$$DFT[u_3] = \sum_{k=0}^{N-1} f[k] e^{-i\frac{6\pi}{N}k}. \quad (37)$$

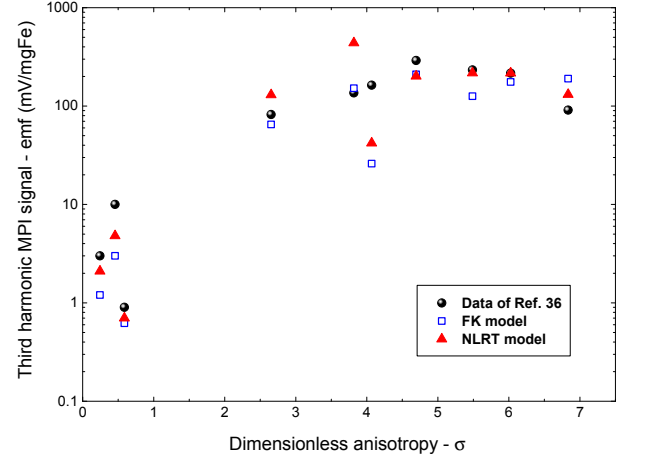


Figure 5. (Color online) MPI third harmonic signal of magnetite-based magnetic fluids containing nanoparticles of different sizes as a function of σ . The figure shows the experimental data (circles) from Ref. [38], calculations using the FK model of Ref. [38] (squares) and the NLRT (triangles) calculation.

The function $f[k]$ is obtained using $f[t] = \frac{\partial M(t)}{\partial t}$ and the time discretization as $t = \frac{k}{Nf_0}$, where f_0 is the excitation field frequency and N corresponds to the number of intervals discretized within one period. In this work $N = 40$. In NLRT model the complete magnetization expression is unknown, so we only use the terms up to the third harmonic. On the other hand, for the FK model, one can expand the Langevin expression up to any order.

Figure 5 we shows the experimental MPI data of the third harmonic magnetization signal of magnetite nanoparticles of distinct sizes performed at 250 kHz (see Ref. [38] for details). Spheres correspond to experimental data, while squares are related to the FK model of Ref. [38]. Note the logarithmic scale and that we are presenting the data in terms of σ . Here we assumed the bulk magnetic anisotropy value, although is well known that the anisotropy is size dependent [40, 49–51]. Nevertheless, size dispersity was taken into account. The calculations used a relaxation time valid for any σ [15, 35] and parameters from Table 1 of Ref. [38]. Triangles correspond to our polydisperse calculation taking the Discrete Fourier Transform and using Eq. (35) in units of V/g, i.e. taking into account in the calculation of $\mathbf{emf}_{3\omega_0}$ the amount of magnetic material in mass per unit volume. Note that our model represents better the MPI experimental data. Indeed from 10 data points NLRT is in better agreement with 80% of the data. Better theoretical results might be achievable if the anisotropy of each sample is known, or even more if one is able to take into account possible particle-particle interaction effects due to agglomerate formation [52]. So, it might be fair to say that, both hyperthermia and MPI experiments seem to be more adequately described by the NLRT model.

Finally, it might be relevant to comment that there is a huge interest of not only deliver heat using magnetic nanoparticle hyperthermia, but also, monitor non-invasively heat delivery using magnetic nanoparticles. In order to be successful in such area, analytical expressions, as the ones derived in this work, that better represent the non-linear response of magnetic nanoparticles, are highly needed. The authors believe that the model developed here might indicate a useful approach towards this important clinical goal.

VI. CONCLUSION

In conclusion, a nonlinear response model of magnetic nanoparticles valid for single-domain nanoparticles was developed. The model is valid beyond the linear response theory, and showed good agreement with dynamic hysteresis simulations using the stochastic Landau-Lifshitz-Gilbert approach and experimental hyperthermia data for field amplitudes as high as 10% of the magnetic anisotropy field. In particular, a generalized expression for the magnetization and the heat loss efficiency (SLP) were obtained. The model showed many features found experimentally in magnetic hyperthermia and MPI studies. As for example, Stoner-Wohlfarth-like dynamic hysteresis curves, distinct SLP field exponents, optimum hyperthermia nanoparticle size shift, among others. The magnetization expression was critically compared with the ones used in MPI and MNT, from which we were able to identify when some approximations can be used. Moreover, the NLRT was found to be valid mostly within the hyperthermia therapeutic window, which suggests strong applicability in the biomedical field.

The authors would like to thank financial support from the Brazilian agencies CNPq, CAPES, FAPEG, FAPESP (2014/01218-2), FAPDF and FUNAPE.

* Corresponding author: mscarriao@ufg.br

- [1] T. Hoare, J. Santamaria, G. F. Goya, S. Irusta, D. Lin, S. Lau, R. Padera, R. Langer, and D. S. Kohane, *Nano Lett.* **9**, 3651 (2009).
- [2] H. Huang, S. Delikanli, H. Zeng, D. M. Ferkey, and A. Pralle, *Nat. Nanotechnol.* **5**, 602 (2010).
- [3] S. Toraya-Brown, M. R. Sheen, P. Zhang, L. Chen, J. R. Baird, E. Demidenko, M. J. Turk, P. J. Hoopes, J. R. Conejo-Garcia, and S. Fiering, *Nanomed.-Nanotechnol. Biol. Med.* **10**, 1273 (2014).
- [4] T. Kobayashi, K. Kakimi, E. Nakayama, and K. Jimbow, *Nanomedicine* **9**, 1715 (2014).
- [5] H. F. Rodrigues, F. M. Mello, L. C. Branquinho, N. Zufelato, E. P. Silveira-Lacerda, and A. F. Bakuzis, *Int. J. Hyperthermia* **29**, 752 (2013).
- [6] C. L. Dennis and R. Ivkov, *Int. J. Hyperthermia* **29**, 715 (2013).
- [7] I. Hilger, R. Hergt, and W. A. Kaiser, *IEE Proc-Nanobiotechnol.* **152**, 33 (2005).
- [8] K. Maier-Hauff, F. Ulrich, D. Nestler, H. Niehoff, P. Wust, B. Thiesen, H. Orawa, V. Budach, and A. Jordan, *J. Neuro-Oncol.* **103**, 317 (2011).
- [9] R. K. Gilchrist, R. Medal, W. Shorey, R. C. Hanselman, J. C. Parrot, and C. B. Taylor, *Ann. Surg.* **146**, 596 (1957).
- [10] M. L. Etheridge and J. C. Bischof, *Ann. Biomed. Eng.* **41**, 78 (2013).
- [11] W. J. Atkinson, I. A. Brezovich, and D. P. Chakraborty, *IEEE Biomedical Engineering BME-31*, 70 (1984).
- [12] P. Debye, *Polar Molecules* (Chemical Catalog, New York, 1929).
- [13] R. Hergt, W. Andrä, C. G. d'Ambly, I. Hilger, W. Kaiser, U. Richter, and H.-G. Schmidt, *IEEE Trans. Magn.* **34**, 3745 (1998).
- [14] R. E. Rosenzweig, *J. Magn. Magn. Mater.* **252**, 370 (2002).
- [15] L. C. Branquinho, M. S. Carrião, A. S. Costa, N. Zufelato, M. H. Sousa, R. Miotto, R. Ivkov, and A. F. Bakuzis, *Sci. Rep.* **3**, 2887 (2013).
- [16] J. Carrey, B. Mehaoui, and M. Respaud, *J. Appl. Phys.* **109**, 083921 (2011).
- [17] E. L. Verde, G. T. Landi, M. S. Carrião, A. L. Drummond, J. A. Gomes, E. D. Vieira, M. H. Sousa, and A. F. Bakuzis, *AIP Adv.* **2**, 032120 (2012).
- [18] E. L. Verde, G. T. Landi, M. H. Sousa, and A. F. Bakuzis, *J. Appl. Phys.* **111**, 123902 (2012).
- [19] R. Richert and S. Weinstein, *Phys. Rev. Lett.* **97**, 095703 (2006).
- [20] A. E. Glazounov and A. K. Tagantsev, *Phys. Rev. Lett.* **85**, 2192 (2000).
- [21] J. L. García-Palacios and P. Svedlinth, *Phys. Rev. Lett.* **85**, 3724 (2000).
- [22] G. T. Landi and A. D. Santos, *J. Appl. Phys.* **111**, 07D121 (2012).
- [23] W. F. J. Brown, *Phys. Rev.* **130**, 1677 (1963).
- [24] P.-M. Déjardin and Y. P. Kalmykov, *J. Appl. Phys.* **106**, 123908 (2009).
- [25] G. T. Landi, *J. Appl. Phys.* **111**, 043901 (2012).
- [26] I. S. Poperechny, Y. L. Raikher, and V. I. Stepanov, *Phys. Rev. B* **82**, 174423 (2010).
- [27] G. T. Landi, *Phys. Rev. B* **89**, 014403 (2014).
- [28] G. Bertotti, *IEEE Trans. Magn.* **24**, 621 (1988).
- [29] R. Hiergeist, W. Andrä, N. Buske, R. Hergt, I. Hilger, U. Richter, and W. Kaiser, *J. Magn. Magn. Mater.* **201**, 420 (1999).
- [30] K. M. Krishnan, *IEEE Trans. Magn.* **46**, 2523 (2010).
- [31] B. Gleich and J. Weizenecker, *Nature* **435**, 1214 (2005).
- [32] P. W. Goodwill, E. U. Saritas, L. R. Croft, T. N. Kim, K. M. Krishnan, D. V. Schaffer, and S. M. Conolly, *Adv. Mater.* **24**, 3870 (2012).
- [33] J. B. Weaver, A. M. Rauwerdink, and E. W. Hansen, *Med. Phys.* **36**, 1822 (2009).
- [34] J. Zhong, W. Liu, L. Kong, and P. C. Morais, *Sci. Rep.* **4**, 6338 (2014).
- [35] W. T. Coffey and Y. P. Kalmykov, *J. Appl. Phys.* **112**, 121301 (2012).
- [36] A. S. Eggeman, S. A. Majetich, D. Farrell, and Q. A. Pankhurst, *IEEE Trans. Magn.* **43**, 2451 (2007).
- [37] A. Tomitaka, K. Ueda, T. Yamada, and Y. Takemura, *J. Magn. Magn. Mater.* **324**, 3437 (2012).

- [38] R. M. Ferguson, K. R. Minard, A. P. Khandhar, and K. M. Krishnan, .
- [39] Y. L. Raikher and V. I. Stepanov, *Phys. Rev. B* **55**, 15005 (1997).
- [40] A. F. Bakuzis and P. C. Morais, *J. Magn. Magn. Mater.* **226-230**, 1924 (2001).
- [41] M. H. Sousa, G. J. da Silva, J. Depeyrot, F. A. Tourinho, and L. F. Zara, *Microchem. J.* **97**, 182 (2011).
- [42] D. E. Bordelon, C. Cornejo, C. Grüttner, F. Westphal, T. L. DeWeese, and R. Ivkov, *J. Appl. Phys.* **109**, 124904 (2011).
- [43] I. Andreu and E. Natividad, *Int. J. Hyperthermia* **29**, 739 (2013).
- [44] S. Ruta, R. Chantrell, and O. Hovorka, *Sci. Rep.* **5**, 9090 (2015).
- [45] P. Jönsson, T. Jonsson, J. L. García-Palacios, and P. Svedlindh, *J. Magn. Magn. Mater.* **222**, 219 (2000).
- [46] Y. L. Raikher and V. I. Stepanov, *J. Magn. Magn. Mater.* **320**, 2692 (2008).
- [47] Y. L. Raikher and V. I. Stepanov, *Phys. Rev. E* **83**, 021401 (2011).
- [48] F. Shubitidze, K. Kekalo, R. Stigliano, and I. Baker, *J. Appl. Phys.* **117**, 094302 (2015).
- [49] F. Bødker, S. Mørup, and S. Linderoth, *Phys. Rev. Lett.* **72**, 282 (1994).
- [50] A. F. Bakuzis, P. C. Morais, and F. A. Tourinho, *J. Magn. Reson. Ser. A* **122**, 100 (1996).
- [51] A. F. Bakuzis, P. C. Morais, and F. Pelegri, *J. Appl. Phys.* **85**, 7480 (1999).
- [52] A. F. Bakuzis, L. C. Branquinho, L. L. Castro, M. T. A. Eloi, and R. Miotto, *Adv. Colloid Interface Sci.* **191-192**, 1 (2013).